4. P. Huybrechts, *Ann. Glaciol.* **10**, 226 (1996).
5. A. Ohmura and N. J. Reeh, *J. Glaciol.* **37**, 140 (1991).
6. Accumulation estimates from recent cores were provided by R. Bales, pending completion of a paper updating the accumulation map for Greenland.
7. C. Davis, personal communication.
8. Values of *T* north of latitude 70°N shown in Fig. 3 are about 4 cm/year lower than our earlier estimates (*2*), reflecting improvement in estimates of snow-accumulation rates resulting from recent investigations.
9. P. Huybrechts, *Global Planet. Change* **9**, 39 (1994).
10. C. H. Davis, C. A. Kluever, B. J. Haines, *Science* **279**, 2086 (1998).
11. W. Krabill *et al.*, *Science* **283**, 1522 (1999).
12. W. Krabill *et al.*, *Science* **289**, 428 (2000).
13. J. McConnell, R. Arthern, E. Mosley-Thompson, C. Davis, R. Bales, paper presented at the Millennium Conference on Earth, Planetary and Solar System Sciences, Nice, France, 25 to 29 April 2000.
14. We thank all who helped with the acquisition and processing of the velocity-traverse data, P. Huybrechts for his model results, J. Finnbogason, who piloted the Twin Otter aircraft used to visit survey stations, and R. Bindschadler for his swift yet thorough review of both this report and its companion (*12*). This project forms part of the Program for Arctic Regional Climate Assessment (PARCA) and was supported by NASA's Polar Research Program and ICESAT Project.

1 March 2000; accepted 7 June 2000

Greenland Ice Sheet: High-Elevation Balance and Peripheral Thinning

W. Krabill,[1]* W. Abdalati,[2] E. Frederick,[3] S. Manizade,[3] C. Martin,[3] J. Sonntag,[3] R. Swift,[3] R. Thomas,[3] W. Wright,[1] J. Yungel[3]

Aircraft laser-altimeter surveys over northern Greenland in 1994 and 1999 have been coupled with previously reported data from southern Greenland to analyze the recent mass-balance of the Greenland Ice Sheet. Above 2000 meters elevation, the ice sheet is in balance on average but has some regions of local thickening or thinning. Thinning predominates at lower elevations, with rates exceeding 1 meter per year close to the coast. Interpolation of our results between flight lines indicates a net loss of about 51 cubic kilometers of ice per year from the entire ice sheet, sufficient to raise sea level by 0.13 millimeter per year—approximately 7% of the observed rise.

The mass balance of the Greenland Ice Sheet is of considerable importance to global sea level, yet there is uncertainty as to whether the ice sheet as a whole is increasing or decreasing in size. Recent advances in airborne laser altimetry and global positioning system (GPS) technology have made possible large-scale assessment of elevation change characteristics of the entire ice sheet through repeat surveys separated in time by several years. Such repeat surveys in 1993 and 1998 (*1*) showed that the southeast margin of the Greenland Ice Sheet has been thinning. Here, we report results from similar measurements in the north of Greenland (1994–99) and provide an assessment of the mass balance of the entire ice sheet.

In 1993 and 1994, NASA's Airborne Topographic Mapper (ATM) measured ice-surface elevations with root mean square (rms) accuracy of 10 cm or better (*1–3*), within a 140-m swath beneath the aircraft, along flight lines crossing all the major ice drainage basins. Ten flight lines from June and July 1993 were resurveyed in June and July 1998 (*1*), and 12 from May and June 1994 were resurveyed in May 1999. For computational efficiency, data from each survey were resampled to 70-m planes (or platelets) that best fit the data acquired on each side of the aircraft (*1*). Elevation changes (dH/dt) for most of the ice sheet were determined by comparing elevation differences at the midpoints between platelet centers from the different years, accounting for the elevation slopes in each platelet (Fig. 1). The comparisons were made only for platelets located within 100 m of each other. Nearer the coast, where the surface becomes too rough to be well fit by planes, the elevation of each laser footprint from the second survey was compared with elevations of all footprints from the first survey lying within a 1-m horizontal radius.

Above 2000 m surface elevation, most of the northern ice sheet lies above the region of summer melting; in the south, there is melting over much of the ice sheet above 2000 m, but most of the meltwater percolates into underlying snow and refreezes. North of 70°N, $|dH/dt|$ is less than 10 cm/year, and spatial variability is low (Fig. 2). By contrast, the area to the south has high spatial gradients, and $|dH/dt|$ reaches 20 cm/year or more. This difference may be associated with lower snow-accumulation rates in the north and comparatively low temporal variability, compared to high snowfall and high temporal variability in the south (*4*). However, the large areas of significant thickening in the south lie in areas where both ice cores (*5*) and model predictions (*4*) show reduced snowfall during the 1990s. This is consistent with results from satellite radar measurements showing higher rates of thickening between latitudes 65° and 68°N from 1978 to 1988 (*6*) and suggests longer term thickening in this area.

The effects of thickening are closely balanced by those of thinning to yield average thickening rates for the ice sheet above 2000 m of 14 ± 7 mm/year in the north and -11 ± 7 mm/year in the south, and 5 ± 5 mm/year for the entire region. Bedrock uplift, estimated to average 4 mm/year in the south and 5 mm/year in the north (*7*) with unknown errors, decreases the average thickening rate to zero. The resulting estimate of $1 \pm >5$ mm/year average thickening for the entire region above 2000 m is close to the estimate of -2 ± 7 mm/year for approximately the same region derived independently by comparing total snow accumulation within the region with total ice discharge from it (*8*).

Below 2000 m surface elevation, the coastal regions are more sparsely covered by flight lines. However, it appears that thinning predominates along approximately 70% of the coast. This applies both to flight lines along and across the direction of ice flow. Thickening regions also exist, but generally at lower rates than areas that are thinning. One exception is the isolated ice cap in the extreme northeast, which is thickening by about 0.5 m/year. Snow accumulation here is strongly influenced by the North East Water polynya, an area of open water surrounded by sea ice. The period between our surveys included 2 years with exceptionally large polynyas, in contrast to the 2 years before with smaller than normal polynyas (*9*). Consequently, the ice-cap thickening is probably a response to locally increased snowfall.

In order to extend our estimates to the edge of the ice sheet in areas not bounded by our surveys, we calculated a hypothetical thinning rate at the coast on the basis of the coastal positive degree day (PDD) anomalies (Fig. 1) (*10*), using a factor of 9 mm per PDD (*11*). We then interpolated between this calculated coastal thinning rate and nearest observed elevation changes to yield thinning rates within the ice-covered coastal regions shown in Fig. 1 (*12*). This approach only considers melt near the coast and neglects the contribution of dynamic thinning. As such, it is a minimum estimate. The total net reduc-

[1]Laboratory for Hydrospheric Processes, NASA Goddard Space Flight Center and [3]EG&G Services, Wallops Flight Facility, Building N-159, Wallops Island, VA 23337, USA. [2]Laboratory for Hydrospheric Processes, NASA Goddard Space Flight Center, Building 33, Room A225, Greenbelt, MD 20771, USA.

*To whom correspondence should be addressed. E-mail: krabill@osb1.wff.nasa.gov

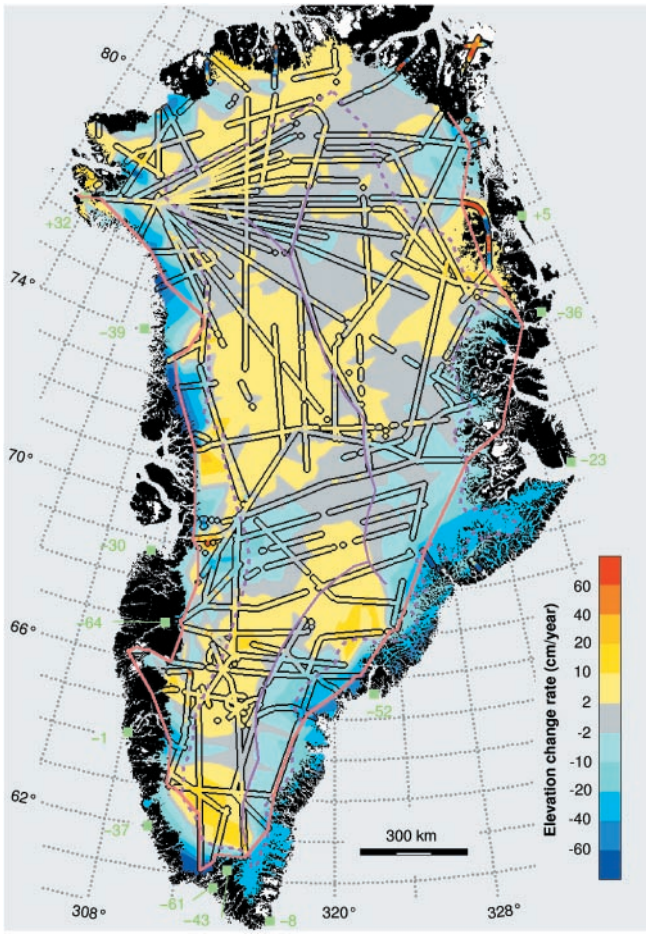

Fig. 1. Greenland, showing flight tracks (outlined in black) of laser-altimeter surveys color-coded according to the rate of change in surface elevation (*dH*/*dt*). Pale gray segments are in balance within the survey errors (±2 cm/year). Regional values of *dH*/*dt* were obtained over most of the ice sheet by interpolating between flight-track data. In areas near the coast (outside the pink boundary) that were not bounded by survey data, we interpolated between flight-track data and hypothetical values of *dH*/*dt* derived from PDD anomalies at coastal weather stations (*10*). The 13 coastal stations are shown in green along with the *dH*/*dt* (cm/year) values derived from the PDD anomalies. The lines of major ice-sheet ridges are shown in violet, and the 2000-m elevation contour is marked by a violet dashed line.

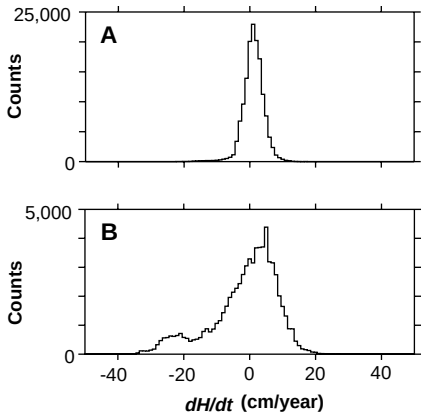

Fig. 2. Histograms of interpolated *dH*/*dt* above 2000-m surface elevation. (**A**) North of 70°N. (**B**) South of 70°N.

tion in ice volume associated with the interpolated values of *dH*/*dt* was 51 km^3/year, which is equivalent to 0.13 mm/year sea-level rise, or about 7% of the observed rate of sea-level increase (*13*). Although we are unable to assign errors to this estimate, we believe that it represents a lower bound for the reasons stated above.

We do not have a satisfactory explanation for the observed, widespread thinning at elevations below 2000 m. Although conditions between 1993–94 and 1998–99 were warmer than the 20-year average (*14*), increased melting and/or reduced snow accumulation cannot explain more than about 50 cm/year of the observed thinning (less in most areas), unless recent summer temperatures were far higher than those that provided equilibrium conditions for the low-elevation parts of the ice sheet. This would require that these equilibrium temperatures were significantly lower than those measured since 1979. However, the most recent colder period ended in the late 1800s (*15*), and Greenland temperature records from 1900–95 (*16*) show highest summer temperatures in the 1930s, followed by a steady decline until the early 1970s and a slow increase since. The 1980s and early 1990s were about half a degree cooler than the 96-year mean. Consequently, if present-day thinning is attributable to warmer temperatures, thinning must have been even higher earlier this century, with total near-coastal thinning of 100 m or more along most of the coast. To some extent, this scenario is supported by historical data (*17*) indicating widespread glacier retreat since the 1800s. However, thinning rates exceeding 1 m/year on many of the glaciers during the survey period are probably too large to be explained in this way, leaving a change in ice dynamics as the most likely cause. Increased creep rates in the lower reaches of the glaciers, and therefore increased discharge velocities, would cause the ice to thin. For example, a typical glacier with thickness of 1000 m would require an increase in longitudinal creep rates by 0.001/year to cause a thinning rate of 1 m/year. If sustained over a distance of 50 km, this would increase discharge velocities by 50 m/year. We have no evidence for such changes, and we cannot explain why they should apply to many glaciers in different parts of Greenland.

References and Notes

1. W. Krabill *et al.*, *Science* **283**, 1522 (1999).
2. Instrument performance was checked each flight by calibration measurements while on the ground and surveys of calibration sites. Comparison of derived ice-surface elevations at all flight-line crossing points for the same year gives rms differences of about 10 cm (*3*), and some of these differences represent real changes during the 3 to 4 weeks of the survey period. However, assuming these differences to be totally caused by errors that are systematic to a flight, all elevation changes inferred along any one flight line could include a bias of 10 cm, or 2 cm/year, which is independent of the biases for other flight lines. Interpolation between flight lines increases the error, but this is offset to some extent by the inclusion of many flight lines and also the independence of errors in different parts of the ice sheet. Over higher elevation parts of the ice sheet, *dH*/*dt* has low spatial variability and there are many flight lines, so interpolated values should have similar errors to those measured along flight lines. Consequently, errors for *dH*/*dt* averaged over large areas of higher elevation ice sheet are approximately $\pm 2/N^{0.5}$ cm, where N is the number of flight lines over the region. Nearer the coast, spatial variability increases and interpolation errors can predominate. Errors that are systematic to an entire year's survey are caused mainly by uncertainty (of about 1 cm) in the location of GPS base stations, introducing a possible bias to estimates of *dH*/*dt* of 0.3 cm/year.
3. W. Krabill, R. H. Thomas, C. F. Martin, R. N. Swift, E. B. Frederick, *Int. J. Remote Sens.* **16**, 1211 (1995).
4. D. H. Bromwich, Q-s. Chen, Y. Li, R. I. Cullather, *J. Geophys. Res.* **104**, 22103 (1999).
5. J. R. McConnell, E. Mosley-Thompson, D. H. Bromwich, R. C. Bales, J. D. Kyne, *J. Geophys. Res.*, **105**, 4039 (2000).
6. C. H. Davis, C. A. Kluever, B. Haines, *Science* **279**, 2086 (1998).
7. J. Wahr, personal communication.
8. R. H. Thomas *et al.*, *Science* **289**, 426 (2000).
9. L. Toudal Pedersen, personal communication. The polynya size was calculated using passive microwave-derived ice concentration data.
10. PDD anomalies were calculated using 6-hourly temperature data dating back to 1979 from coastal stations around the perimeter of Greenland. Of the 54 stations in the data set, the 13 shown in Fig. 1 had values for at least 15 of the last 20 years, and for all five of the years that separate the surveys. Anomalies were calculated by subtracting the mean PDD for the full record from that for the 5-year period between surveys.
11. The PDD ablation factors used are 3 mm water/PDD for snow and 8 mm water/PDD for ice [R. J. Braithwaite, *J. Glaciol.* **41**, 153 (1995)]. After adjusting for density, each of these numbers corresponds to an elevation change of 9 mm/PDD.
12. Interpolation in coastal areas excluded measured *dH*/*dt* values outside the boundary in Fig. 1 (often extreme thinning along glaciers); instead, it used bilinear interpolation between ice sheet measurements and the conservative PDD-derived values. The

area influenced by the coastal stations is mostly in the south and comprises 10.5% of the ice sheet area, and accounted for −38.5 km³/year volume change (75% of the total). The true volume change in this area is likely to be greater.

13. R. Warrick, C. Le Provost, M. Meier, J. Oerlemans, P. Woodworth, in *Climate Change, 1995: The Science of Climate Change* (Cambridge Univ. Press, Cambridge, 1996), pp. 359–405.
14. Temperature records were decoded by the National Center for Environmental Prediction and were obtained from the National Center for Atmospheric Research.
15. M. M. Herron, S. L. Herron, C. C. Langway, *Nature* **293**, 389 (1981).
16. A temperature record for 1900–95 was calculated using data from the NOAA National Climate Diagnostic Center accessible at http://www.ncdc.noaa.gov/onlineprod/ghcnmcdwseasonal/form.html. Quality control procedures are described in J. K. Eischeid *et al.* [*J. Appl. Meteorol.* **34**, 2787 (1995)].
17. A. Weidick, *Rapp. Gronlands Geol. Unders.* **152**, 73 (1991).
18. We thank the crew of the NASA P-3 aircraft used for the Greenland surveys. We acknowledge the technical support of R. Mitchell, A. Waller, and J. Scott. This work was supported by NASA's Polar Research Program and the ICESAT Project.

2 March 2000; accepted 7 June 2000

Stability of Ferropericlase in the Lower Mantle

L. S. Dubrovinsky,[1]* N. A. Dubrovinskaia,[1] S. K. Saxena,[1] H. Annersten,[1] E. Hålenius,[1] H. Harryson,[1] F. Tutti,[1] S. Rekhi,[1] T. Le Bihan[2]

We have heated ferropericlases $(Mg_{0.60}Fe_{0.40})O$ and $(Mg_{0.50}Fe_{0.50})O$ to temperatures of 1000 kelvin at pressures of 86 gigapascals, simulating the stability of the solid solution at physical conditions relevant to Earth's lower mantle. The in situ x-ray study of the externally heated samples in a Mao-Bell–type diamond anvil cell shows that ferropericlase may dissociate into magnesium-rich and iron-rich oxide components. The result is important because the decomposition of ferropericlase into lighter and heavier phases will cause dynamic effects that could lead to mantle heterogeneity.

Ferropericlase (Mg,Fe)O and $(Mg,Fe)SiO_3$-perovskite are considered to form the bulk of Earth's lower mantle. Therefore, ferropericlase $[(Mg_{1-x}Fe_x)O, x \leq 0.5]$ and magnesiowüstite $[(Mg_{1-x}Fe_x)O, x > 0.5]$ have been studied extensively (*1–14*). At ambient conditions, the end members of the MgO-FeO solid solution—periclase (MgO) and wüstite (FeO)—have the same halite NaCl (B1) structure, and they form a complete solid solution. However, at pressures above 17 GPa and ambient temperature (*15*), wüstite transforms to a phase with rhombohedral structure (*16*). With increasing pressure above 100 GPa at 300 K, it transforms to the NiAs (B8) or the anti-NiAs (a-B8) structure (*7, 12, 13*), whereas periclase retains the NaCl structure at least to 227 GPa (*11*). The NaCl structure is based on cubic close packing of the anions, but the B8 (or the a-B8) structure is formed by hexagonal close packing of the anions (or cations). The topological difference between the B8 and B1 structures at high pressure could lead to an immiscibility gap in the region of the MgO-FeO solid solution (*17*). To investigate this hypothesis, we conducted an in situ high-pressure, high-temperature study of ferropericlase with two intermediate compositions, $(Mg_{0.6}Fe_{0.4})O$ and quenched $(Mg_{0.5}Fe_{0.5})O$, respectively.

Experiments were performed on beamline ID30 at ESRF (Grenoble, France) and at the Uppsala Lab in Sweden (*18*). Samples, synthesized as described in (*1*), were externally heated in a Mao-Bell–type diamond anvil cell (*15*). The powder samples of ferropericlase were loaded into a hole (initial diameter 70 to 75 μm) in a Re gasket, which was then confined between beveled diamonds with 200-μm culets. Pressure was determined by using powdered platinum (99.999% purity) as an in situ x-ray standard mixed in small proportion (~5 volume %) with the ferropericlase samples. For the analysis of the integrated x-ray spectra, we used the programs GSAS (*19*) and PeakFit 4.0 (Figs. 1 and 2). The lattice parameter of Pt was determined with a precision better than 0.002 Å over the whole pressure and temperature range studied, resulting in an uncertainty of 2 GPa at pressures up to 80 GPa. At ambient conditions, the lattice parameters of ferropericlase are 4.2627(6) Å (numbers in parentheses are standard deviations in the last significant digits) for $(Mg_{0.6}Fe_{0.4})O$ and 4.2716(7) Å for $(Mg_{0.5}Fe_{0.5})O$. These values agree with previous data (*1, 2, 4*). Rietveld refinements yielded occupancies for the metal position of Fe 0.38(3) and Mg 0.62(3) in $(Mg_{0.6}Fe_{0.4})O$ and Fe 0.52(4) and Mg 0.48(4) in $(Mg_{0.5}Fe_{0.5})O$.

In our experiments with ferropericlase $(Mg_{0.6}Fe_{0.4})O$, we first increased the pressure at ambient temperature to 47 ± 1 GPa (*15*) (Fig. 1) and then increased the temperature to 950 to 980 K. This heating further raised the pressure to 61 ± 2 GPa. The sample was heated for 4 hours, during which no changes were observed except for a slight asymmetric broadening of the (220) reflection. Then the pressure was increased to 86 ± 2 GPa at a temperature of 975 ± 5 K (*15*), and after 5 to 6 hours of heating, all the reflections of ferropericlase became asymmetric and some showed splitting (Figs. 1 to 3). It was not possible to describe the diffraction pattern assuming only a mixture of cubic ferropericlase and platinum (Fig. 2A). A mixture of three phases [platinum, cubic, and rhombohedral ferropericlases in the proportion 1:22:3 (Fig. 2B)] had to be assumed to reproduce all features of the pattern. Cubic ferropericlase (Fig. 2B) had a molar volume of 8.68(1) cm³/mol, corresponding to a pressure of 84 ± 2 GPa at 970 K according to the equation of state for $(Mg_{0.6}Fe_{0.4})O$ (*4*). The molar volume of the rhombohedral phase (Fig. 2B) at the same condition is 9.20(1) cm³/mol. The thermal equation of state of rhombohedral ferropericlase is unknown. Using available data (*4, 5, 16*), we estimated the bulk modulus at ambient conditions, $K_{300,0}$, to lie between 150 and 160 GPa, its pressure derivative $K' = 4$, and dK/dT between −0.01 and −0.025 GPa/K. The observed molar volume V_0 of 9.20 cm³/mol at 85 GPa and 970 K would indicate a molar volume of 12.14 to 12.31 cm³/mol at ambient conditions. These values correspond to the volume of stoichiometric cubic wüstite (*2, 20*). Upon decompression, the reflections of ferropericlase remained split (Fig. 1). The quality of the diffraction patterns of the quenched samples was not good enough for Rietveld refinement, but the x-ray data of the quenched samples at ambient conditions showed the presence of two cubic phases with lattice parameters of 4.253(1) and 4.327(1) Å, respectively. The first corresponds to a ferropericlase with the composition 35 atomic % FeO and 65 atomic % MgO, and the second to an almost stoichiometric pure wüstite (*2, 20*). The lattice parameters of platinum matched the initial value before the experiments [$a = 3.9231(5)$ Å] within experimental error (0.0004 Å). Within the limit of error (~3%), no ferric iron was detected by Mössbauer spectroscopy in the ferropericlase before and after our experiments (*21*).

In the experiments with ferropericlase $(Mg_{0.5}Fe_{0.5})O$, we heated the sample for 5 to 6 hours between 950 and 1000 K at four different pressures: 56(3), 67(3), 74(4), and 83(5) GPa

[1]Institute of Earth Sciences, Uppsala University, S-752 36 Uppsala, Sweden. [2]European Synchrotron Radiation Facility (ESRF), BP 220, F-38043 Grenoble Cedex, France.

*To whom correspondence should be addressed.